Astron. Astrophys. 333, 287–297 (1998)

ASTRONOMY AND ASTROPHYSICS

SiO shocks in the L 1157 molecular outflow⋆

F. Gueth[1], **S. Guilloteau**[1], **and R. Bachiller**[2]

[1] Institut de Radio Astronomie Millimétrique, 300 rue de la Piscine, F-38406 Saint Martin d'Hères, France
[2] Observatorio Astronómico Nacional (IGN), Apartado 1143, E-28800 Alcalá de Henares, Spain

Received 30 July 1997 / Accepted 22 December 1997

Abstract. We report high angular resolution IRAM Plateau de Bure interferometric observations of the SiO $v = 0$ J $= 2 \rightarrow 1$ and J $= 5 \rightarrow 4$ transitions in the southern lobe of the young L 1157 molecular outflow. The resolution of these observations ($\sim 2.5''$) makes them directly comparable to available high-resolution CO maps of the flow. The known precession of the L 1157 flow is fully confirmed. We find a remarkable morphological agreement between the strong SiO shocks revealed by these observations and the two CO cavities of the southern lobe of the outflow: the positions, shapes and opening angles are similar in both tracers, with the SiO emission ahead of or at the edges of the CO emission. Each CO cavity is associated with a shock which is placed exactly at its apex and exhibits a linear feature pointing exactly towards the protostellar position. The CO appears in the wake of these leading shocks. These coincidences, as well as the presence of two independent shock/cavity systems, strongly support shock-entrainment models for the formation of molecular outflows.

These observations also provide detailed information on the internal structure of the shocked regions. They confirm that a strong enhancement of the SiO abundance occurs within shocks. The comparison with high-angular resolution images of other shock-tracers (NH_3, H_2) shows that chemical and evolution effects play a crucial role in the observed brightness distributions. The SiO velocity distribution is mainly forward, but the kinematics seems to result from both the complex formation processes of SiO and the velocity field produced by bow-shocks. Finally, we briefly discuss the apparent density structure of the shocks, and especially the possible origin of the linear precursor seen downstream from the main bow-shock.

Key words: ISM: individual objects: L 1157 – ISM: jets and outflows – ISM: molecules – radio lines: ISM – stars: formation – shock waves

1. Introduction

Several physical mechanisms have been proposed to explain the formation of molecular outflows (see e.g. Cabrit et al. 1997). Swept-up shells driven by wide-angle winds focussed by a stratified ambient molecular medium (e.g. Li & Shu 1996) can account for some of the observed properties of molecular outflows (Cabrit et al. 1997), but there is now increasing evidence that a large fraction of the flows, and especially the highly-collimated outflows, are driven by jets originating from the central protostars (see e.g. Bachiller 1996). A high-velocity jet can put into motion ambient molecular gas through the formation of a steady-state turbulent mixing layer along its edges, created e.g. by Kelvin-Helmholtz instabilities (e.g. Cantó & Raga 1991; Stahler 1994; Taylor & Raga 1995). The predicted resulting lobes are extremely narrow. Alternatively, prompt entrainment models have been proposed (e.g. Raga & Cabrit 1993; Masson & Chernin 1993; Chernin et al. 1994), in which the jet entrains the ambient gas through the propagation of large bow-shocks which occur at the head and/or within the jet, at the location of velocity discontinuities. These bows are able to disturb the gas over large transverse distances and the outflow is then identified with the wake of the bow-shock(s).

High-resolution mm interferometry is a powerful tool to investigate the very first steps of the formation of molecular outflows, since detailed comparison between observations and predictions from theoretical models become possible. In this framework, a very promising source is located in the L 1157 molecular cloud, at a distance of 440 pc. This extremely young molecular outflow is excited by a Class 0 source of $L_{\rm bol} \sim 11\,L_\odot$ (IRAS 20386+6751, or L 1157-mm; see Gueth et al. 1997). Despite this low luminosity, the southern (blueshifted) lobe of the flow exhibits particularly important signs of shock excitation through strong emission in several molecular lines (Umemoto et al. 1992; Mikami et al. 1992; Davis & Eislöffel 1995; Avery & Chiao 1995; Tafalla & Bachiller 1995; Bachiller et al. 1995b). Very recently, Gueth et al. (1996) have completely mapped this lobe in the CO J $= 1 \rightarrow 0$ line with high resolution ($\sim 3''$) interferometric observations. These images reveal two large structures (labeled C1 and C2) with a strong density contrast between the walls and the inner parts. The two cavities are not aligned on the same line passing through the central protostar, strongly suggesting a *precession* of the ejection direction (see Fig. 1).

A very exciting characteristic of the L 1157 outflow is its strong SiO emission (Mikami et al. 1992). The SiO molecule is one of the most interesting shock tracers in molecular outflows

Send offprint requests to: F. Gueth

⋆ Based on observations performed with the IRAM Plateau de Bure interferometer.

(e.g. Martín-Pintado et al. 1992), since it is thought to be *formed* in shocks: grain destruction releases gas-phase silicon, which is then rapidly oxydized to produce SiO (e.g. Flower et al. 1996; Schilke et al. 1997). The SiO emission is thus specifically tracing the shocked gas. In the blueshifted lobe of the L 1157 flow, the SiO abundance is enhanced by at least four orders of magnitude (Mikami et al. 1992; Avery & Chiao 1995). Zhang et al. (1995) have mapped this part of the flow in the SiO J $= 2 \rightarrow 1$ line with $\sim 9''$ resolution, showing the clumpy structure of the emission. In this paper, we present high-resolution ($\sim 2.5''$) interferometric images of the blueshifted lobe of L 1157 in the SiO $v = 0$ J $= 2 \rightarrow 1$ and J $= 5 \rightarrow 4$ rotational transitions. These maps allow an accurate comparison between the CO and the SiO emission, i.e. between a tracer of the flow itself and a tracer of the shock structure. They also provide detailed information on the internal structure of the shocks.

2. Observations and results

2.1. Interferometric observations

The SiO J $= 2 \rightarrow 1$ interferometric observations were carried out in January-March 1994 with the IRAM interferometer at Plateau de Bure (Guilloteau et al. 1992). A mosaic of three fields was performed to cover the southern part of the flow (Fig. 1). Four configurations of the 4 antenna array were used, with baselines extending up to 290 m. The antennas were equipped with SIS receivers with typical SSB system temperatures of about 150 to 220 K at the SiO J $= 2 \rightarrow 1$ frequency. We used a spectral correlator configured to give 256 channels of 0.078 MHz separation (0.27 km s^{-1} at 86 GHz). Phase and amplitude calibrations were achieved by observations of the quasar 2021+614. Typical rms phase noise was lower than 20°. The flux density scale was derived from the observations of 2021+614, whose flux (0.7 Jy, accurate to $\sim 10\%$) was determined relative to 3C273. In addition to the SiO line, we also used one of the correlator units to observe the $H^{13}CO^+$ J $= 1 \rightarrow 0$ line. No emission was however detected in the observed fields. The data were calibrated and analyzed with the GILDAS package developed at IRAM and Observatoire de Grenoble. The SiO mosaic was deconvolved using a generalization of the CLEAN algorithm to mosaics. The clean beam is $2.8'' \times 2.2''$ at PA 56°.

Observations of the SiO J $= 5 \rightarrow 4$ line were obtained in September 1995. Only the most compact configuration of the 4 antenna array was used, with baselines up to 64 m. The receivers provided typical SSB system temperature between 300 and 350 K at the SiO J $= 5 \rightarrow 4$ frequency. The spectral correlator was configured to give 128 channels of 0.625 MHz separation (i.e. 0.86 km s^{-1} at 217 GHz). Phase and amplitude calibrations were done relative to 1823+568, whose flux was fixed to 1.85 Jy. The observations were carried out in excellent weather conditions, and the phase noise was lower than 15°. Only one field was observed, almost in a central position in the flow (see Fig. 1). Note that the primary beam of the interferometer is only 23″ at 217 GHz. The SiO J $= 5 \rightarrow 4$ image was deconvolved using the classical CLEAN algorithm: the final clean beam is $3.4'' \times 2.9''$ at PA 56°.

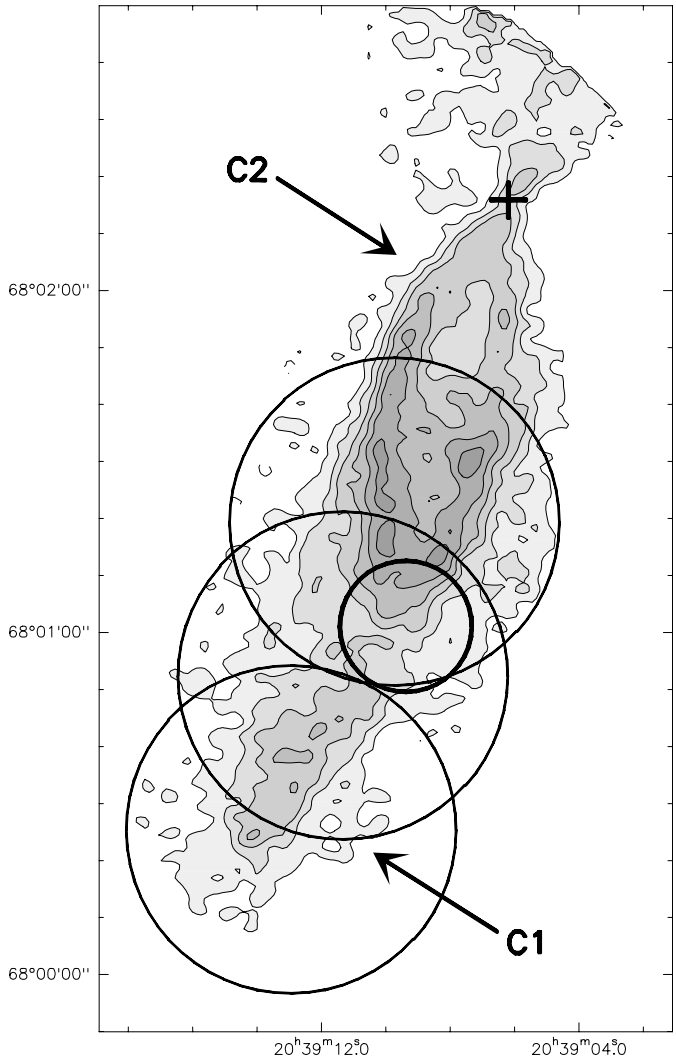

Fig. 1. Location of the fields mapped in SiO J $= 2 \rightarrow 1$ (thin circles) and J $= 5 \rightarrow 4$ (thick circle). The half-power primary beams are superimposed on the integrated CO J $= 1 \rightarrow 0$ emission (from Gueth et al. 1996) in greyscale. Contours are -1.5 then 0.75 to 8.25 by 1.5 Jy km s^{-1}/beam. The clean beam is $3.6'' \times 3''$ at PA 90°. C1 and C2 indicate the cavities referred by Gueth et al. (1996). The cross indicates the positions of the protostar L1157-mm, at $20^h39^m06^s.19$, 68°02′15″.9 (J2000.0), as measured with the λ 2.7 mm continuum emission (Gueth et al. 1997).

Figs. 2 and 3 present the channel maps of the two SiO transitions. To provide easier comparison with the SiO J $= 2 \rightarrow 1$ mosaic, the SiO J $= 5 \rightarrow 4$ images have been corrected from the primary beam attenuation.

2.2. Results

The SiO J $= 2 \rightarrow 1$ emission is split in three main structures, labeled S1 to S3 in Fig. 2, among which the strongest emission is associated with a clear bow-shaped shock S2. The southern part of S3 is seen as a high-velocity "bullet", i.e. as a small feature detected up to large velocities, with a morphology almost similar

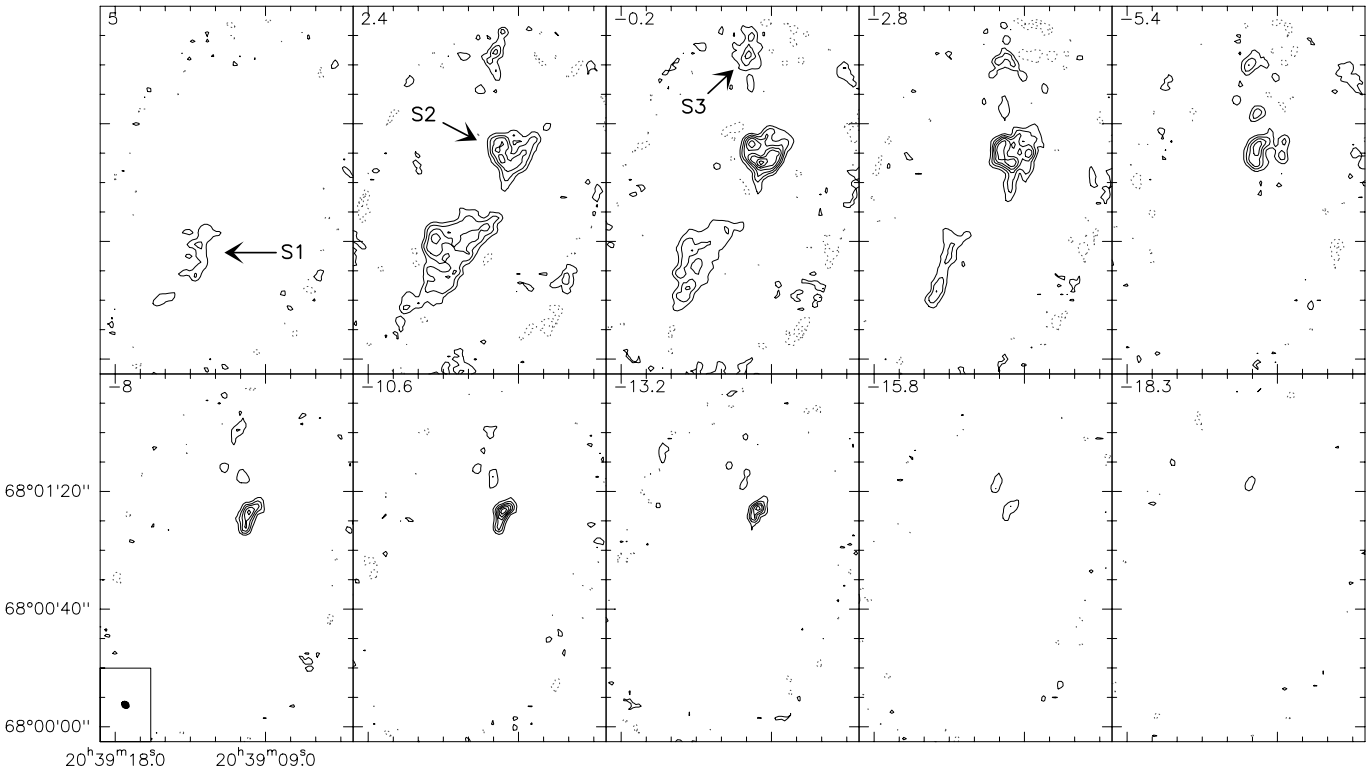

Fig. 2. Channel maps of the SiO J $= 2 \rightarrow 1$ emission, integrated over velocity intervals of 2.6 km s^{-1} wide. The central LSR velocity for each interval is indicated in the upper left corner of each panel. The systemic velocity of L 1157 is 2.6 km s^{-1} (Gueth et al. 1997). First contour and step are 55 mJy/beam (1.45 K), approximately 3σ. The clean beam is $2.8'' \times 2.2''$ ($\simeq 1200 \times 1000$ AU) at PA 56° and is drawn in the first panel of the second line. Note that the mosaic is corrected from primary beam attenuation, and the noise thus strongly increases at the edges of the field of view.

in all channels. The observations presented in Fig. 2 are in good agreement with the lower resolution data of Zhang et al. (1995), but do not show the western extensions of S1 and S2 seen in these previous observations; we presume these extensions were due to remaining sidelobe artifacts in the maps of Zhang et al. (1995).

Comparison between the integrated SiO J $= 2 \rightarrow 1$ and CO J $= 1 \rightarrow 0$ emission (Fig. 4) reveals an extremely good agreement. The S1 and S2 SiO shocks are exactly at the positions and have the same shapes and opening angles as the extremities of the C1 and C2 cavities. S3 consists of two filaments which coincide with the edges of the two CO cavities. Even some fine morphological details are reproduced in both tracers, such as the asymmetry of S1/C1, which are brighter towards the West, or the bar-like transverse structure in C2, whose eastern part is visible in S3.

Another striking feature revealed by these observations is that both S1 and S2 show linear sub-structures: S1 appears as a linear "jet" in one channel map ($V_{lsr} = -2.8$ km s^{-1}), whereas S2 exhibits a small linear extension downstream. These two linear features are not only pointing almost exactly towards the central protostar, but also correspond to the axis of the two CO cavities (Fig. 4, right panel).

The S2 shock was also observed in the SiO J $= 5 \rightarrow 4$ transition (Fig. 3). The observed field was centered on the linear feature detected ahead of S2 in the SiO J $= 2 \rightarrow 1$ maps. Fig. 3 shows that the S2 structure is globally similar in the two SiO transitions: a clearly bow-shaped emission, with its eastern part brighter and detected up to larger velocities than the western part, and a linear sub-structure just ahead of the bow. The velocity range of the emission is also almost the same in both transitions.

3. Shock entrainment in a precessing jet

3.1. Precession

In a previous paper (Gueth et al. 1996) we developed a spatio-kinematical model of the L 1157 outflow, in which the two CO cavities are supposed to have been created by the propagation of two independent ejection events. Precession of the ejection direction by about 6° around a mean inclination of $\sim 10°$ to the plane of the sky provides a common explanation for the different orientations and velocities of the C1 and C2 cavities. C1 is almost in the plane of the sky (inclination of $\sim 3°$) and C2 is in a West elongation, towards us. The observations presented here provide additional support for this scenario, since the SiO emission reveals strong shocks located at the apex of the two CO cavities, with the same misalignment. Moreover, the SiO maps show two linear structures aligned along the cavity axes and intersecting at the protostellar condensation (Fig. 4),

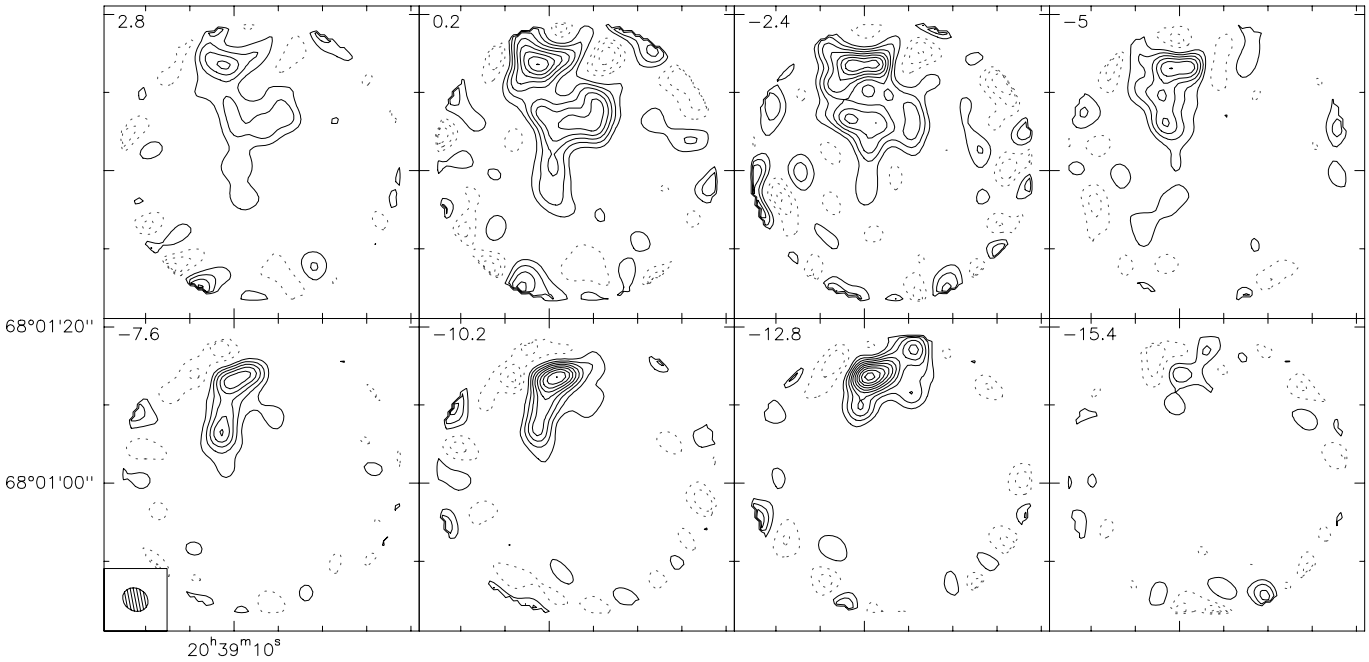

Fig. 3. Channel maps of the SiO J $= 5 \rightarrow 4$ emission, integrated over velocity intervals of 2.6 km s^{-1} wide. The central LSR velocity for each interval is indicated in the upper left corner of each panel. First contour and step are 150 mJy/beam (0.4 K). The clean beam is $3.4'' \times 2.9''$ ($\simeq 1500 \times 1250$ AU) at PA 56° and is drawn in the first panel of the second line. The primary beam attenuation (modelled by a gaussian of $23''$ FWHM) has been corrected. As a consequence, the noise distribution strongly increases at the edges of the maps, that we have truncated to give a field of view of $38''$.

as expected if the two SiO shocks are propagating in different directions traced by part of the SiO emission. Finally, the velocity range of S1 is redshifted in comparison to S2, in agreement with the proposed geometry (S1/C1 closer to the plane of the sky than S2/C2). The projection angles derived from the precession model yield dynamical ages of ~ 3000 and ~ 2000 years for S1 and S2, assuming a constant shock propagation velocity $V_S = 100$ km s^{-1}.

Although it cannot be ruled out that the SiO shocks correspond to completely decoupled ejection events, the almost continuous structure revealed by the integrated emission (Fig. 4) suggests that the ejection phenomenon is rather continuous. The overall structure of the L 1157 outflow makes actually quite appealing a picture in which the SiO shocks are travelling down in an underlying, precessing jet. In this case, S1 would be the terminal shock against the interstellar medium, whereas S2 would have been created by density and/or velocity variation in the jet (see e.g. Raga 1993; Raga & Cabrit 1993). Precession of the ejection direction can also favor the creation of internal shocks within a jet (Raga & Biro 1993).

The precession model provides a qualitative explanation for some of the morphological aspects of the SiO emission. The 3-dimensional picture of the flow reveals that the two CO cavities are overlapping, and that S2 has travelled within the walls of the C1 cavity. It is thus not surprising to find the strongest shock associated with S2. The asymmetry of S1/C1 can also be qualitatively understood, since between S1 and S2 the jet has precessed towards the West, thus encountering and shocking the western part of the molecular gas. A similar explanation can be put forward for S3, since here the jet has precessed towards the East, and produced an oblique shock with the edge of the C1 and C2 cavities. S3 also corresponds to the region where the two CO cavities overlap each other.

The precession of the ejection direction of the L 1157 outflow is confirmed by observations of the northern lobe of the flow in CO J $= 2 \rightarrow 1$ (Bachiller & Pérez Gutiérrez 1997): S1, S2, and S3 have corresponding features towards the North, with the same misalignments. The northern part of the flow is however more extended and weaker than the southern one, suggesting it is expanding in a less dense medium.

3.2. Shock entrainment

The remarkable agreement between the S1 and S2 SiO shocks and the associated CO cavities gives strong observational support to the idea that molecular outflows are created through the propagation of large bow-shocks (e.g. Raga & Cabrit 1993; Masson & Chernin 1993; Chernin et al. 1994). In particular, shock-entrainment models provide a simple explanation (the propagation of two independent shocks) for the presence of two distinct shock/cavity systems, which can hardly be explained in a "continuous" wind or steady-state picture.

The S2 shock associated with the C2 CO cavity is a striking example of the association between a bow-shock structure and a CO molecular outflow. Despite its asymmetry, S2 has a very clear U-shape. The walls of the C2 cavity are just in the elongation of the bars of the U, i.e. *in the wake of the shock*. This corresponds exactly to the identification between the molecular

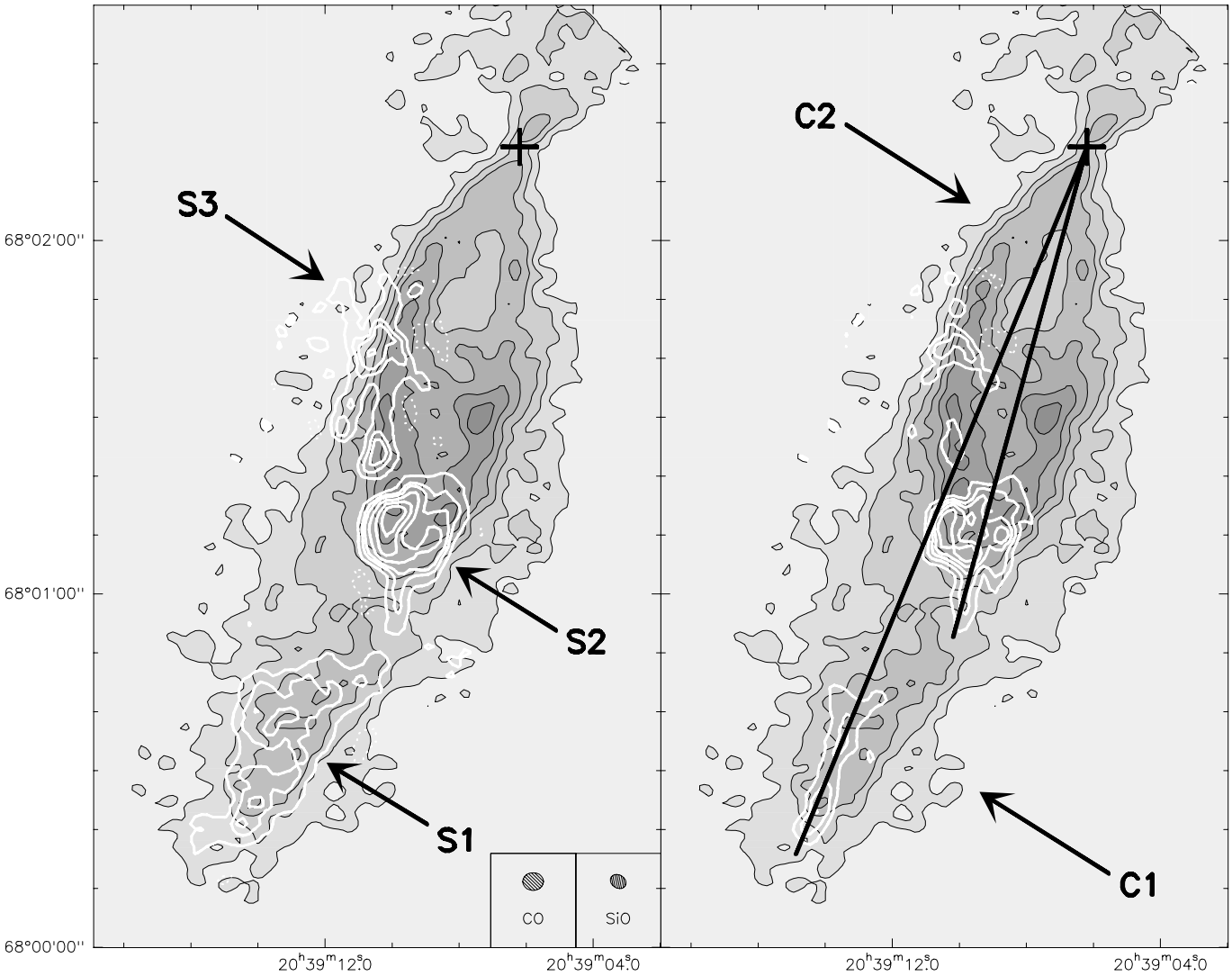

Fig. 4. *(Left)* Overlay of the integrated CO J $= 1 \rightarrow 0$ (greyscale) and SiO J $= 2 \rightarrow 1$ (white contours) emission. For the CO map, contours are -1.5 then 0.75 to 8.25 by 1.5 Jy km s^{-1}/beam, and the clean beam is $3.6'' \times 3''$ at PA 90°. For the SiO map, contours are -0.4, 0.3, 0.8, 1.2, 2, 3, 4 Jy km s^{-1}/beam, and the clean beam is $2.8'' \times 2.2''$ at PA 56°. *(Right)* Overlay of the integrated CO J $= 1 \rightarrow 0$ and the SiO J $= 2 \rightarrow 1$ emission at LSR velocity -2.8 km s^{-1} (integrated over an interval of 2.6 km s^{-1} wide). The SiO contour step is 55 mJy/beam, as in Fig. 2. In both panels, the cross indicates the position of the protostar L1157-mm. For clarity, the outer regions of the SiO image, where the noise level is quite high, have been masked. Note that the northern part of the flow, near the protostar, has not been observed in the SiO line.

outflow and the wake of the leading shock, proposed e.g. by Raga & Cabrit (1993).

The apparent displacement between the SiO and CO emission at the S2 shock location (SiO is observed ahead of CO) can be attributed to several effects, such as CO dissociation on the shock axis, temperature gradients, or SiO abundance variations. To be able to compare the shape of the flow cavity with predictions from simple analytic models (which do not take into account the above effects), one should consider the envelope merging the SiO bow-shock and the CO cavity. The resulting shape is then in good agreement with the simulations presented by Raga & Cabrit (1993; see their Fig. 2, case $\beta = -2$). Numerical 3-D simulations presented by Smith et al. (1997) predict limb-brightened CO cavities in the wake of the leading shock, which resembles the C2/S2 system. However, these simulations do not reproduce the complete CO cavities which are observed up to the central protostar in L 1157.

4. Properties of the SiO emission

4.1. The SiO shocks

The observations reported in this paper confirm that the SiO abundance is strongly enhanced in the shocks that are taking place in the L 1157 flow (see paragraph 6.1). The three main shocks in the blueshifted lobe of L 1157 have linear sizes of the order of 10^4 AU. Their aspects are however rather different. Whereas S1 and S2 are likely to be leading shocks propagating in the interstellar medium, S3 is most probably a region of

interaction between the CO cavities and/or with the underlying jet. Its morphology is accordingly rather complex.

S2 has a clear bow shape, which remains more or less similar between V_{lsr} 2.4 and -2.8 km s^{-1} (Figs. 2 and 3). Only its bright eastern part is visible at higher (blueshifted) velocities. This strong asymmetry indicates that the actual nature of S2 is probably even more complex than a single bow-shock. We further discuss below (paragraph 6.2) the nature of the linear precursor of S2.

The terminal shock S1 is less bright and more extended than S2. There is no clear bow shape, but a more collimated V-shape. This qualitative difference with the S2 shock could be due either to an intrinsic difference (e.g. external densities) between the terminal shock against the interstellar medium (S1) and an internal shock within the jet (S2), or to an evolution effect in the shock structure, since S1 is older than S2. Numerical simulations presented by Suttner et al. (1997) actually predict an evolution in the shape of the bow-shocks, which become more collimated with time. Another striking feature in S1 is the linear structure seen at $V_{lsr} = -2.8$ km s^{-1} (Figs. 2 and 4), as if part of the SiO emission was directly linked with the underlying jet at this position.

Finally, it should be pointed out that the S2 shock is propagating in a medium which has already been processed by the passage of S1. The chemical content of the pre-shock ambient gas could thus have been modified: SiO may already be present in a significant amount and/or the dust composition may be affected. This could have strong effects on the chemical processes taking place within the shock and thus affect the resulting SiO emission.

4.2. Comparison with other shock tracers

The southern lobe of L 1157 has been mapped at high angular resolution in two other shock-tracers: NH_3 (Tafalla & Bachiller 1995) and H_2 (Hodapp 1994; Davis & Eislöffel 1995). Fig. 5 presents the resulting images, together with the CO and SiO integrated emission.

The NH_3(3,3) emission (observed with $\sim 5.5''$ resolution) shows extremely good morphological agreement with the SiO $J = 2 \rightarrow 1$ map, even in some fine details such as substructures in the S1 shock. The only significant difference is the lack of NH_3 emission at velocities below -6 km s^{-1}, while SiO is detectable up to -18 km s^{-1}, but this can be due to differences in sensitivity. It is thus likely that the two lines are tracing very similar physical conditions. The kinetic temperature derived from multi-line ammonia observations is ~ 80 K (Tafalla & Bachiller 1995).

The H_2 2.12 μm line emission has a quite different behaviour. H_2 emission is detected near the S2 and S3 shocks (which are also seen through the Hα and [SII] lines[1], Devine et al. 1997). However, no H_2 emission is detected at the S1 position. This suggests this shock is colder than S2, either because it is weaker (S1 is a shock against the interstellar medium whereas S2 is probably travelling in the dense walls of C1) or because it is older and thus corresponds to a later evolutionary stage of the shock physics (see also Zhang et al. 1995, who discuss the possibility of higher extinction).

To properly compare the observed morphologies in the S2/S3 region, we carefully checked the astrometry of the images presented in Fig. 5. The positional uncertainties in the interferometric CO $J = 1 \rightarrow 0$ and SiO $J = 2 \rightarrow 1$ maps are below $\sim 0.4''$. Davis & Eislöffel (1995) announced a position accuracy of $\sim 1''$ in their image. We also considered the H_2 emission map presented by Hodapp (1994), for which we derived a coordinate system with an accuracy about $0.4''$ from the positions of 20 field stars found in the STScI Digitized Sky Survey. The images of Hodapp and Davis & Eislöffel are then in agreement within $\sim 1.5''$, as expected. We thus conclude that the relative positional uncertainties between the millimeter and infrared images presented in Fig. 5 are below $1.5''$.

Fig. 6 presents an overlay of the H_2, CO, and SiO brightness distributions. The H_2 emission is clearly confined in the *inner* part of the cavity excavated by the shock propagation. The main H_2 structure appears upstream of the S2 shock and exhibits the opposite asymmetry. These differences must be due to the SiO and NH_3 not tracing the same physical conditions as the H_2 2.12 μm line. The kinetic temperature derived from ammonia observations, ~ 80 K, is much lower than the temperature required to excite the ro-vibrational lines of H_2.

If the main H_2 shock is the counterpart of S2, then the SiO emission is located downstream from the H_2 emission. This situation is also found in the outflow driven by the extremely young source IRAS 03282+3035 (Bachiller et al. 1994). This could be the signature of a complex shock structure, in which an extended magnetic precursor (e.g. Draine & McKee 1993) allows SiO to be formed before a J-shock, in which the temperature reaches the high value needed to excite the H_2 line. This configuration is actually what is suggested by the time-dependent calculations presented by Pineau des Forêts et al. (1997).

Because of the jet precession, the above interpretation is unfortunately not unique. The axis of the H_2 emission shows a slight misalignment with the C2/S2 axis (Fig. 6). In the precession model, this would indicate that the H_2 emission is actually associated with a later position of the jet than S2 (which corresponds to the western elongation of the ejection axis) and thus to a younger evolutionary stage of the shock physics. In this interpretation, it is interesting to note that the high velocity SiO bullet detected between S2 and S3 (see Fig. 2) is co-located with or even upstream of the main H_2 shock. This configuration would imply a strong J-shock exciting H_2 lines, followed by a cooling region in which SiO can be formed.

Finally, the bright knot of the H_2 emission (noted A_5 in Davis & Eislöffel 1995) at the South-East from the main shock has no counterparts in any of the other tracers (Figs. 5, 6) and thus remains difficult to interpret.

In any case, the complex interrelations between the H_2, NH_3 and SiO brightness distributions show that the different shock-

[1] The detection of the strong S2/S3 shock in the Hα and [SII] lines makes it fully identifiable as an Herbig-Haro object. It is now included as HH 375 in the general catalogue of HH objects.

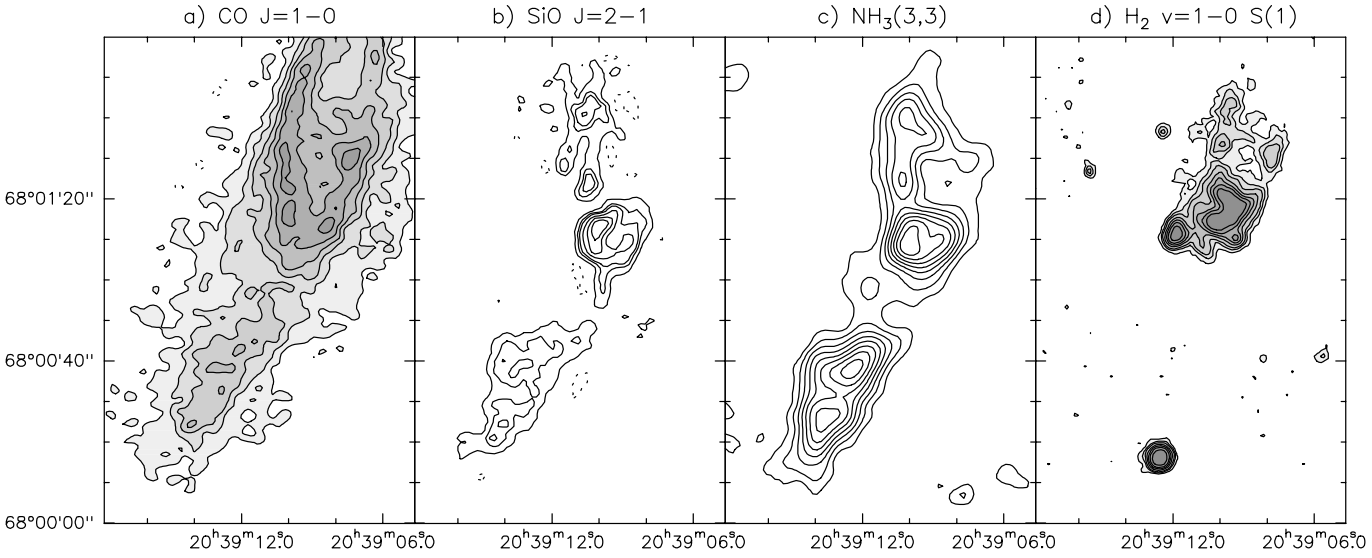

Fig. 5. High-resolution images of the molecular emission through the blueshifted lobe of the L 1157 molecular outflow. **a** Integrated CO J $= 1 \rightarrow 0$ emission (see Fig. 1 and 4). Resolution is $3.6'' \times 3''$. **b** Integrated SiO J $= 2 \rightarrow 1$ emission (see Fig. 4). Resolution is $2.8'' \times 2.2''$. **c** Integrated NH_3(3,3) emission (from Tafalla & Bachiller 1995). Resolution is $5.8'' \times 5.1''$. **d** H_2 v=1–0 S(1) + continuum emission (from Davis & Eislöffel 1995). Resolution is around $1.5''$. The strong point-like emission at the southern edge of the map is a field star.

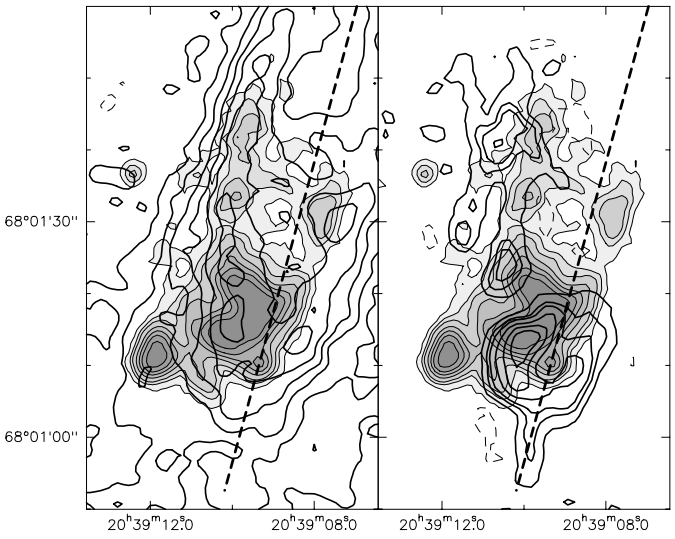

Fig. 6. Overlay of the H_2 v=1–0 S(1) + continuum emission in greyscale (from Davis & Eislöffel 1995) and the CO J $= 1 \rightarrow 0$ (left) and SiO J $= 2 \rightarrow 1$ (right) integrated emission in the S2/S3 region. The dashed line is the axis of the C2 cavity indicated in Fig. 4.

tracer emission are affected not only by temperature but also by chemical and evolution effects (see also Bachiller & Pérez Gutiérrez 1997). Detailed shock models taking into account H_2 emission as well as shock-induced chemistry are required to properly interpret these observations.

4.3. Comparison with other SiO outflows

SiO emission has been detected in only a few extremely young molecular outflows (e.g. Martín-Pintado et al. 1992; Chandler & Richer 1997). Among them, only the L 1448 flow has been mapped so far at high angular resolution in SiO line(s) (Guilloteau et al. 1992; Dutrey et al. 1997; see also Bachiller et al. 1995a). In this object, the SiO J $= 2 \rightarrow 1$ line traces a highly collimated, clumpy, jet-like structure which coincides with the axis of the CO flow. It is terminated by a strong bow-shock (Dutrey et al. 1997).

The SiO emission in L 1448 and L 1157 thus present some similarities: in both cases, SiO is tracing strong shocks but also appears more closely associated with the underlying jet (the linear features in S1 and S2 in the L 1157 case). Differences also exist: the SiO emission is seen all along the jet in the L 1448 case, whereas it is concentrated in a few well-developed shocks in L 1157. The lack of high-angular resolution CO data for the whole L 1448 flow unfortunately precludes detailed comparison between the CO and SiO emission in this object.

We note that preliminary results on the extremely young HH 211 flow (Chandler & Richer 1997; Gueth et al. unpublished observations) indicate that the SiO emission in this object presents yet another behaviour: SiO seems to trace a continuous jet-like structure, without any emission at the position of the strong terminal shocks.

High angular resolution images of more objects are thus needed to assess a reliable picture of the "SiO flows" phenomenon and to distinguish between individual particularities and (probably strong) evolution effects in the apparent SiO emission morphology.

5. SiO velocity distribution

Given the complexity of a bow-shock structure as well as of the physical mechanisms leading to the formation of SiO in shocks, to derive deprojected velocities from the observations

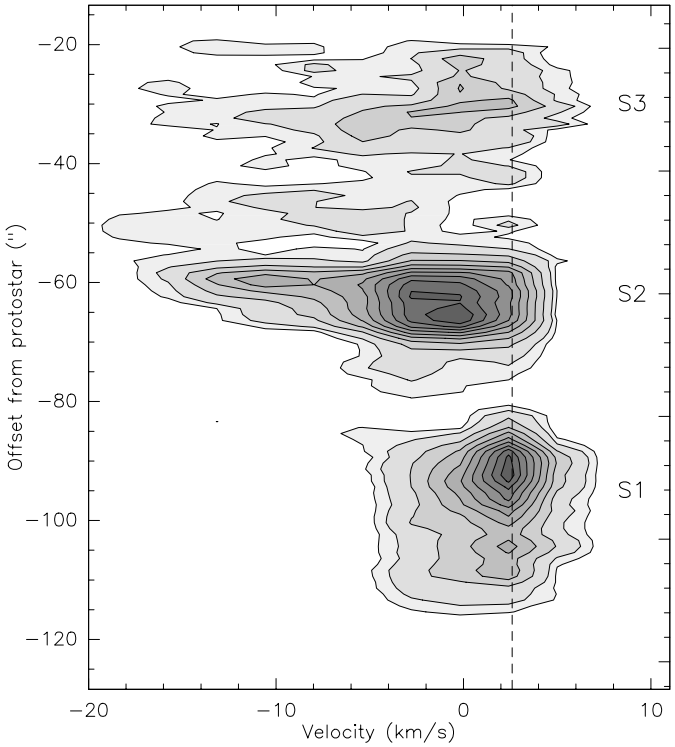

Fig. 7. Position-velocity diagram of the SiO J $= 2 \rightarrow 1$ emission, computed along the north-south (i.e. declination) axis and integrated over the transverse dimension. The systemic velocity of L 1157 is 2.6 km s^{-1} and is indicated as a dashed vertical line. Contours are 5% then 10% to 90% by 10% of the maximum. Note the low velocity resolution (2.6 km s^{-1}, as in Fig. 2).

is a rather difficult step. In addition, the L 1157 flow is very close to the plane of the sky, and the velocity range in which the SiO shocks can be observed is accordingly scaled down. Moreover, the presence of the bright eastern spot in S2 can be misleading in properly analysing the spectra and morphology of this shock. Hence, the velocity dependence of the morphological aspects of the observed shocks in L 1157 are not reproduced by simple bow-shock models (as e.g. Hartigan et al. 1987 or Dutrey et al. 1997).

Fig. 7 presents a position-velocity diagram of the SiO J $= 2 \rightarrow 1$ emission, computed along the jet axis. Apart from the strong eastern part of S2, which is seen as a large wing towards high negative velocities, few details appear in the structure of the shocks. This has most probably to be related to the low inclination angle to the plane of the sky of L 1157.

We briefly discuss in the following two aspects of the observed velocity distribution. We shall mainly discuss S1 and S2, which are likely to be leading (bow) shocks propagating in the interstellar medium.

5.1. SiO kinematics in the shocks

Schilke et al. (1997) have modeled the formation of the SiO molecule in C-type shocks, in the context of molecular outflows. These theoretical considerations indicate that the shock velocity must exceed ~ 20 km s^{-1} to allow SiO to be formed, and be lower than ~ 60 km s^{-1} to avoid the shock to become dissociative.

The simulations presented by these authors yield typical sizes for the regions traced by the SiO emission which correspond to the L 1157 case. However, the synthetic spectra disagree with the velocity distributions observed in L 1157. The model profiles have a maximum at the highest velocities and a gradual wing towards the ambient velocity. Such behaviour is observed in the closest SiO bullets from the L1448 protostar (Schilke et al. 1997), but in the L 1157 case, neither S1 nor S2 display such asymmetries. The strong S2 shock even exhibits the opposite profile.

Schilke et al. (1997) have only considered the case of a face-on plane-parallel shock front. However, the SiO formation rate depends on the effective shock velocity, and is thus expected to vary along the surface of a bow-shock. This effect, combined with projection and/or opacity effects in the bow geometry and to obvious very strong projection effects in the L 1157 flow (which is almost in the plane of the sky) may strongly affect the observed velocity distribution and thus preclude any meaningful comparison between simple models and the observations.

5.2. Forward motions

For simplicity, let us consider only the velocity distribution expected in a bow-shock, independently from the specific SiO chemistry that we thus assume to be uniform within the shock.

In both S1 and S2, redshifted emission is detected (see Fig. 7), which requires transverse motions as obtained in bow-shocks to be produced. The bulk of the emission is however blueshifted, which indicates that the velocity field in the bow is mainly forward. However, simple bow-shock models predict a velocity field which is not forward but rather normal to the bow surface[2], resulting in a very strong overlap of red- and blue-shifted emission. This is especially the case for shocks very close to the plane of the sky as in L 1157, and to explain the present observations a mechanism to convert normal motion of the post-shocked gas into a more forward direction is thus needed (see also the discussion of Lada & Fich 1996). This last point has been recently investigated e.g. by Smith et al. (1997), who show that turbulent mixing into the swept-up layer can produce such forward motions (see also Zhang and Zheng 1997, and Wilkin 1996, who solves exactly for the shape and velocity field in a momentum-driven bow-shock). It should be noted that forward velocities can also be obtained with a "simple" bow-shock if it is propagating into ambient gas which is already in motion.

This last hypothesis can easily be tested in the case of the simplified bow-shock model of Hartigan et al. (1987). We note $V_{\rm S}$ the shock propagation velocity, $V_{\rm amb}$ the velocity of the am-

[2] In the shock frame, the component of the ambient gas velocity normal to the bow surface can be assumed to be thermalized while the parallel component is conserved. When coming back to the observer's frame, the resulting velocity vector is then perpendicular to the bow surface (Hartigan et al. 1987; Lada & Fich 1996; Dutrey et al. 1997).

Table 1. Velocities observed and derived for the two shocks S1 and S2 and the two observed SiO transitions. All the velocities are in $\mathrm{km\,s^{-1}}$. The systemic velocity $V_{\rm sys}$ is 2.6 $\mathrm{km\,s^{-1}}$. The angles are negative for an observed lobe pointing towards us.

Shock	S1	S2	S2
SiO line	$J = 2 \rightarrow 1$	$J = 2 \rightarrow 1$	$J = 5 \rightarrow 4$
ΔV	7.8	18.2	18.2
$V_{\rm mean}$	1.1	-6.7	-6.35
i	$-3°$	$-9°$	$-9°$
$V_{\rm S}$	32.5	68.5	66.3
$V_{\rm amb}$	24.7	50.3	48.1

bient pre-shock medium, $V_{\rm sys}$ the systemic velocity, and i the inclination of the shock axis (i.e. of the underlying jet) to the plane of the sky. The velocity dispersion ΔV and the medium velocity $V_{\rm mean}$ of the observed emission (i.e. respectively the difference and the average of the minimal and maximal velocities) are then given by (Hartigan et al. 1987; see also Dutrey et al. 1997):

$$\Delta V = V_{\rm S} - V_{\rm amb} \quad (1)$$

$$V_{\rm mean} = \frac{V_{\rm S} + V_{\rm amb}}{2} \sin i + V_{\rm sys} \quad (2)$$

Since the inclinations are known from the precession model, these relations allow us to recover $V_{\rm S}$ and $V_{\rm amb}$. Table 1 gives the values obtained for S1 and S2.

Considering the restrictive assumptions used to derive Eqs. 1–2, as well as the strong projection effects in L 1157, values given in Table 1 should only be considered as indicative. In particular, the ambient velocity determined ahead of S1 is different from zero, which may indicate that S1 is not the terminal shock. This explanation is in contradiction with the lack of high velocity CO emission further from the protostar. It seems more likely that this simple kinematic analysis does not apply to S1. Note however that a similar problem was found by Dutrey et al. (1997) for L 1448. In the case of S2, where the bow shape is well defined, the analysis indicates pre-shock velocities around 50 $\mathrm{km\,s^{-1}}$. This value is consistent with the idea that S2 is a shock between the jet and the C1 cavity walls (i.e. material already shocked and accelerated).

6. The S2 shock

6.1. Physical conditions

The strong S2 shock has been observed in two SiO rotational transitions, which can in principle be used to perform simple radiative transfer calculations. The results are quite sensitive to the measured flux densities, especially since only two transitions are available. We thus carefully checked whether the interferometric observations have filtered out part of the emission. The SiO $J = 2 \rightarrow 1$ images are most probably free of such instrumental artifacts: the structure is rather small compared to the primary beam, and, even if short-spacings have not been added to the dataset, the total flux of S2 agrees within 10% to the single-dish result of Mikami et al. (1992). On the contrary, the SiO $J = 5 \rightarrow 4$ emission is quite extended compared to the 23″ primary beam of the interferometer. Single-dish measurements performed with the IRAM 30-m (Bachiller & Pérez Gutiérrez 1997) actually show that the interferometric image only recover $\sim 30\%$ of the flux. To estimate the image artifacts, we re-processed the SiO $J = 2 \rightarrow 1$ map in an identical way to the SiO $J = 5 \rightarrow 4$ observations: same 23″ primary beam, same (poor) uv coverage, same deconvolution procedure. The lost flux in this process amounts to up to 70%, and the resulting images show deep absorption in the upper right part of the shock: this could explain the similar feature observed in the SiO $J = 5 \rightarrow 4$ maps.

Assuming the same excitation temperature $T_{\rm ex}$ for the two lines and optically thin emission, one can deduce $T_{\rm ex}$ and the SiO column density from the observed brightness ratios. Accounting for the missed flux in SiO $J = 5 \rightarrow 4$, the derived excitation temperatures vary between 10 and 30 K. This is much lower than the ~ 80 K kinetic temperature derived from ammonia observations (Bachiller et al. 1993; Tafalla & Bachiller 1995). The simplest explanation is that the density is high enough to excite the SiO $J = 5 \rightarrow 4$ transition, but not to thermalize it. This indicates a typical density of order $10^5\,\mathrm{cm^{-3}}$.

The SiO column densities derived from this method range between a few $10^{13}\,\mathrm{cm^{-2}}$ (small linear extension ahead of the shock) and a few $10^{14}\,\mathrm{cm^{-2}}$ (eastern part of the shock, where the emission is the strongest). These numbers are consistent with previously reported values (Mikami et al. 1992; Zhang et al. 1995). From the typical density ($10^5\,\mathrm{cm^{-3}}$) and sizes (a few 1000 AU), we derive H_2 column densities of order $\sim 10^{21}\,\mathrm{cm^{-2}}$ and hence SiO abundances about 10^{-7}. This is at least four orders of magnitude larger than the SiO abundance in typical dark clouds, thus confirming the creation of SiO molecules in the shock.

6.2. Linear precursor

One of the most surprising features detected in the S2 shock is the small linear structure placed just ahead of the bow shape. It is detected between LSR velocities of 2.4 and -2.8 $\mathrm{km\,s^{-1}}$ without any clear evidence of changes from channel to channel (see Fig. 2), and is confirmed by the SiO $J = 5 \rightarrow 4$ observations. Since it is almost exactly pointing away from the protostellar condensation position (Fig. 4, right panel), it is tempting to interpret it as the trace of the underlying jet in which the shock is propagating. However, the clear association between this SiO jet-like feature and S2 suggests that the shock itself is at the origin of the physical mechanism that produces this emission. A similar feature, although less clear, has been reported for the terminal shock in L 1448 (Dutrey et al. 1997; see Fig. 8). We briefly discuss below possible mechanisms that could produce such linear precursors in shocks.

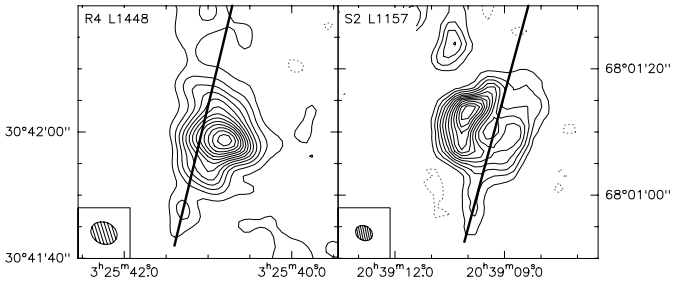

Fig. 8. The R4 shock in L 1448 (from Dutrey et al. 1997) and the S2 shock in L 1157, both observed in the SiO J $= 2 \rightarrow 1$ line. The two shocks exhibit an extension downstream, pointing away from the protostellar positions (thick lines). For the L 1448 image, contours are 0.6 Jy km s^{-1}/beam and the clean beam is $4.2'' \times 3.4''$ at PA 62°. For the L 1157 image, contours are 0.4 Jy km s^{-1}/beam and the clean beam is $2.8'' \times 2.2''$ at PA 56°. In both cases, the beam corresponds to a linear size of ~ 1000 AU.

6.2.1. Density variation?

As indicated above, the 3-D picture of the L 1157 flow indicates that S2 has travelled within the walls of the C1 cavity. The present position of S2 roughly corresponds to the point where it emerges from C1. Strong spatial variation of the ambient density can thus be expected, resulting in important acceleration of part of the shock. The linear precursor of S2 could thus be the trace of such a phenomenon occuring on the jet axis. This explanation is however specific to the L 1157 geometry, and cannot be invoked for the feature observed in the L 1448 molecular outflow.

6.2.2. A magnetic precursor?

The structure of a shock propagating in a weakly-ionized gas is considerably modified by the presence of a (transverse) magnetic field (e.g. Draine 1980; Draine & McKee 1993). The preshock medium can be disturbed before the arrival of the shock front in a so-called magnetic precursor, and the flow variables can even remain continuous (C-type shock) if this precursor is strong enough. The formation of SiO in shocks is actually most easily explained in the framework of C-shocks (e.g. Flower et al. 1996; Schilke et al. 1997; Pineau des Forêts et al. 1997).

However, if the magnetic field is high in the jet alone (e.g. because the jet corresponds to the direction perpendicular to the ambient magnetic field, leading to the maximal effective magnetic induction), one can expect a magnetic precursor to develop preferably within the jet, resulting in an extension of the shock at this place. It is however unclear whether such a complex configuration is viable and if it can account for the formation of the SiO molecules. We note however that SiO could be already present in the jet (or in a cocoon surrounding the jet) or could arise from the previous shock S1, as suggested by the almost continuous emission revealed by the integrated SiO J $= 2 \rightarrow 1$ emission (Fig. 4, left panel). In this case, the precursor would just enhance the density and temperature to provide excitation to the existing molecules.

6.2.3. A "nose cone"?

Another possible explanation for the observed linear structure in S2 is provided by numerical MHD simulations of the propagation of a shock in a jet (Clarke et al. 1986; Lind et al. 1989; Ouyed et al. 1997). One of the features revealed by these simulations is the presence of a so-called "nose cone", i.e. a conical shape of the front part of the shock. The matter between the terminal mach disk in the jet and the leading shock is actually confined by the magnetic field in such a flattened region. Depending on the ratio of thermal to magnetic pressures, the resulting morphologies can be quite different (Lind et al. 1989). Such shocks do not exhibit features as collimated as the linear filament in S2, but rather resemble the conical structure seen in the 2.4 km s^{-1} channel of Fig. 2. Finally, we note that the matter has already been shocked in a nose cone, and the SiO molecules could thus be formed through grain disruption: no other *ad hoc* phenomenon has to be invoked.

7. Conclusions

The high-resolution interferometric observations reported in this paper reveal a wealth of details in the internal structure of a young molecular outflow. Our main results are the following:

1. The SiO rotational transitions in the blueshifted lobe of the L 1157 molecular outflow trace three main shocks, whose morphology presents a remarkable agreement with the CO emission. The position, shapes, opening angles, and many morphological details are similar in both tracers, with the SiO emission ahead of or at the edges of the CO emission. Each of the two CO cavities of the flow is associated with a strong SiO shock placed exactly at its apex. Both shocks exhibit linear sub-structures which point almost exactly towards the central protostar but also coincide with the axis of the CO cavities.
2. These morphological coincidences and the presence of two decoupled shock/cavity systems give strong observational support to shock-entrainment models for the formation of molecular outflows. The S2 SiO shock and the C2 CO cavity are a remarkable example of the association between a bow-shock and a molecular flow, in which the CO emission appears exactly in the wake of the strong shock traced by SiO.
3. The precession of the underlying jet of L 1157-mm, revealed by previous high-resolution CO maps, is fully confirmed by these observations.
4. The comparison between these high-angular resolution SiO images and other shock-tracer observations (NH_3, H_2) reveals the complex structure of the shocked regions. The observed brightness distributions are clearly affected by chemical and evolution effects, but also by the actual nature (e.g. the presence or not of a magnetic precursor) of the shocks.
5. The SiO velocity field most probably results from the complex formation processes of this molecule as well as from the velocity distribution occuring in bow-shocks. Although it is affected by strong projection effects, the observed veloc-

ity field appears to be mainly forward, which indicates that the post-shocked motions are *not* normal to the bow-shock surface.

6. The internal structure of the S2 shock reveals a strong enhancement of the SiO abundance, as well as direct evidence of the density structure of the shock. The SiO emission also reveals a linear "precursor" to the strong S2 shock. Such precursors may be a common feature in jet-driven molecular outflows.

Acknowledgements. We are grateful to the IRAM staff at Plateau de Bure for competent help with the observations. We also thank Drs. S. Cabrit, A. Dutrey, and M. Tafalla for many discussions on outflows. Dr. R. Pudritz kindly called our attention to the possibility of a nose cone. We thank Dr. J. Eislöffel for providing us the H_2 image, and Dr. M. McCaughrean for useful help in analysing the infrared plates. R.B. acknowledges partial support from Spanish DGYCIT Grant PB93-0048.

References

Avery L.W., Chiao M., 1996, ApJ 463, 642
Bachiller R., Martín-Pintado J., Fuente A., 1993, ApJ 417, L45
Bachiller R., Terebey S., Jarrett T., et al., 1994, ApJ 437, 296
Bachiller R., Guilloteau S., Dutrey A., Planesas P., Martín-Pintado J., 1995a, A & A 299, 857
Bachiller R., Liechti S., Walmsley C.M., Colomer F., 1995b, A & A 295, L51
Bachiller R., 1996, ARA & A 34, 111
Bachiller R., Pérez Gutiérrez M., 1997, ApJ 487, L93
Cantó J., Raga A.C, 1991, ApJ 372, 646
Cabrit S., Raga A.C., Gueth F., 1997, in Reipurth B., Bertout C. (eds) Proc. IAU Symp. 182, *Herbig-Haro Flows and the Birth of Low Mass Stars*. Kluwer, Dordrecht, p. 163
Chandler C., Richer J., 1997, in Malbet F., Castets A. (eds) Poster Proc. IAU Symp. 182, *Low Mass Star Formation from Infall to Outflow*, p. 76
Chernin L.M., Masson C. R., Gouveia Dal Pino E. M., Benz W., 1994, ApJ 426, 204
Clarke D.A., Norman M.L., Burns J.O., 1986, ApJ 311, L63
Davis C.J., Eislöffel J., 1995, A & A 300, 851
Devine D., Reipurth B., Bally J., 1997, in Malbet F., Castets A. (eds) Poster Proc. IAU Symp. 182, *Low Mass Star Formation from Infall to Outflow*, p. 91
Draine B.T., 1980, ApJ 241, 1021
Draine B.T., McKee C.F., 1993, ARA & A 31, 373
Dutrey A., Guilloteau S., Bachiller R., 1997, A & A 325, 758
Flower D.R., Pineau des Forêts G., Field D., May P.W., 1996, MNRAS 280, 447
Gueth F., Guilloteau S., Bachiller R., 1996, A & A 307, 891
Gueth F., Guilloteau S., Dutrey A., Bachiller R., 1997, A & A 323, 943
Guilloteau S., Delannoy J., Downes D., et al., 1992, A & A 262, 624
Guilloteau S., Bachiller R., Fuente A., Lucas R., 1992, A & A 265, L49
Hartigan P., Raymond J., Hartmann L., 1987, ApJ 316, 323
Hodapp K., 1994, ApJS 94, 615
Lada C.J., Fich M., 1996, ApJ 459, 638
Li Z.Y, Shu F.H, 1996, ApJ 472, 211
Lind K.R., Payne D.G., Meier D.L., Blandford R.D., 1989, ApJ 344, 89
Martín-Pintado J., Bachiller R., Fuente A., 1992, A & A 254, 315
Masson C.R., Chernin L.M., 1993, ApJ 414, 230
Mikami H., Umemoto T., Yamamoto S., Saito S., 1992, ApJ 392, L87
Ouyed R., Pudritz R.E., Stone J.M., 1997, Nature 385, 409
Pineau des Forêts G., Flower D.R., Chièze J.P., 1997, in Reipurth B., Bertout C. (eds) Proc. IAU Symp. 182, *Herbig-Haro Flows and the Birth of Low Mass Stars*. Kluwer, Dordrecht, p. 200
Raga A.C., Cabrit S., 1993, A & A 278, 267
Raga A.C., 1993, Ap & SS 208, 163
Raga A.C., Biro S., 1993, MNRAS 264, 758
Schilke P., Walmsley C.M., Pineau des Forêts G., Flower D.R., 1996, A & A 321, 293
Smith M.D., Suttner G., Yorke H.W., 1997, A & A 323, 223
Stahler S.W., 1994, ApJ 422, 616
Suttner G., Smith M.D., Yorke H.W., Zinnecker H., 1997, A & A 318, 595
Tafalla M., Bachiller R., 1995, ApJ 443, L37
Taylor S.D., Raga A.C., 1995, A & A 296, 823
Umemoto T., Iwata T., Fukui Y., et al., 1992, ApJ 392, L83
Wilkin F.P., 1996, ApJ 459, 31
Zhang Q., Ho P.T.P., Wright M.C.H., Wilner D., 1995, ApJ 451, L71
Zhang Q., Zheng X., 1997, ApJ 474, 719